

## **19EA Direct Containment Heating**

### **19EA.1 Summary Description**

Direct Containment Heating (DCH) is the sudden heatup and pressurization of containment resulting from the fragmentation and dispersal of core material in the containment atmosphere. DCH is a concern for sequences in which the vessel fails at high pressure since the steam flow from the vessel provides the motive force for entrainment. In the event of a sufficiently large DCH event, the containment could fail at the time of vessel failure. Since this could lead to very high releases to the environment, a study has been carried out to investigate the uncertainties in the challenge to containment due to a DCH event. In the past, this issue has been primarily addressed for Pressurized Water Reactors (Reference 19EA-1) since BWRs have very reliable vessel depressurization systems. Thus, the frequency of accidents with the vessel remaining at high pressure is extremely low.

Subsection 19D.6.2.5 provides an evaluation of the ADS System reliability including the nitrogen, control and instrumentation systems. Additional information about the SRVs and the ADS System may be found in Subsections 5.2.2, 7.3.1.1.1.2 and 19E.2.1.2.2.2.

Subsection 7.3.1.1.1.2(3)(h) indicates that the signal cables, solenoid valves, safety/relief valve operators and accumulators are located inside the drywell and are designed to operate in the most severe accident resulting from a DBA LOCA, including the radiation effects. The conditions in the containment during the early stages of a severe accident (before vessel failure) which require depressurization using the SRVs are less challenging than those specified by a DBA LOCA. Additional analyses of the ADS System capability were performed in support of station blackout performance analysis. This discussion is included in Subsection 19E.2.1.2.2.2. The conclusions of that analysis are that there is ample DC power for the operation of the SRVs for many days after the 8 hour capability required by the station blackout rule.

Subsection 5.2.2.4.1 indicates that the nitrogen accumulator capacity for each valve is designed to be sufficient to open for one actuation at drywell design pressure even if the air supply to the accumulators is lost. The risk significant severe accidents in the ABWR PRA remain below the design pressure of the containment in the time period before vessel failure. Valve operability at high containment pressure conditions are also discussed in Subsection 19E.2.1.2.2.2(2)(b). Based on the presence of the containment overpressure protection system, the maximum drywell pressure is approximately 0.79 MPa (100 psig). Subsection 19E.2.1.2.2.2(2)(b) indicates the operator actions which could be taken to assure SRV operability under these conditions. The appropriate operator actions are specified in the ABWR EPGs. Since the containment pressurizes very slowly, over a period of about a day, there is ample time for the operators to take the appropriate actions.

Given the above discussions, one may conclude that the ADS System will not be compromised before vessel failure in the unlikely event of a severe accident, and the frequency of severe accident sequences in which the vessel fails at high pressure is extremely low. However, with

the many sources of low-pressure injection available to the ABWR to prevent core damage, the frequency of all core damage sequences is very low. Therefore, high-pressure core melts appear as contributors to the total core damage frequency, albeit with a very low probability.

A detailed study utilizing event trees was performed to assess the peak drywell pressure resulting from a DCH event. This attachment outlines the analysis and the results.

## **19EA.2 Description of Event Tree Analysis**

The early containment failure event tree analysis consists of a main tree (Figures 19EA-1, 19EA-2, and 19EA-3) and three supplemental decomposition event trees (DETs) (Figures 19EA-4, 19EA-5, and 19EA-6). The first two events on the main event tree sort the sequence classes by Reactor Pressure Vessel (RPV) pressure and pre-existing containment pressure at the time of vessel failure. These parameters are uniquely determined by the accident class attributes. The last event on the main event tree assesses the probability of drywell head failure following vessel failure. The probabilities for this event are evaluated in supplemental DETs. Three DETs were constructed to assist in the quantification for accident classes with high RPV pressure. (Low RPV pressure sequence classes are not expected to lead to containment pressures which would challenge the integrity of containment.) The three DETs assess the probability of containment failure for different pre-existing containment pressures at the time of RPV failure.

The DETs consider the major phenomena which contribute to early over pressurization of containment from high RPV pressure sequences including debris entrainment from the lower drywell, Direct Containment Heating (DCH), the pre-existing pressure in containment prior to RPV failure, and the pressure rise due to blowdown of the RPV. Each pathway through a DET represents a possible accident progression pathway given the uncertainties in the underlying phenomena. A peak containment pressure is associated with each pathway. These pressures have been estimated from a deterministic DCH model (described in Subsection 19EA.3) with input conditions which reproduce the parameter values and assumptions along each sequence pathway on the tree. These pressures were then compared with the containment fragility curve (developed in Attachment 19FA) to determine the probability of containment failure.

The probabilities for each sequence pathway with similar end states were summed and these results transferred as the branch probabilities for the last event on the main event tree.

The spectrum of pressures and associated probabilities represented by the quantified DETs represents a discrete probability distribution of containment pressurization following vessel failure. This distribution is a representation of the uncertainties associated with the estimation of containment pressurization due to the phenomena occurring at vessel failure.

### **19EA.2.1 Event Headings**

The important parameters and assumptions which are considered as headings on the main event tree and the DETs and the reason for their use are discussed below.

**19EA.2.1.1 Containment Pressure Prior to RPV Failure (CONTPRES)**

The pre-existing pressure of the containment is obviously important in the assessment of containment pressurization following vessel failure. Three pressure regimes have been selected to represent the range of possible pre-RPV failure containment pressures. MAAP-ABWR calculations (described in Subsection 19E.2.2 and summarized on Table 19EA-1) indicate that ABWR accident sequences can be grouped into three classes. These pressure regimes are similar to those selected to represent pre-RPV failure containment pressures in NUREG/CR-4551 (Reference 19EA-2).

<b>Class</b>	<b>Pressure Range</b>	<b>Examples</b>
Low	0.134-0.264 MPa (Nominal = 1.5 atmosphere.)	Non ATWS sequences with operable DHR or with rapid core damage (i.e., all invessel injection failed).
Inter	0.264-0.310 MPa (Nominal = 2.5 atmosphere)	Large LOCAs with early failure of DHR. SBO with RCIC and failure of DHR.
High	>0.310 MPa (Nominal = 4 atmosphere)	ATWS with RCIC.

This event is quantified based on the sequence accident class. This is a sorting type event. The probability of each branch is either 0 or 1 depending upon the attributes of the accident class.

**19EA.2.1.2 RPV Pressure at RPV Failure (RVPRES)**

The RPV pressure at the time of vessel failure is a major parameter impacting a number of processes which contribute to containment pressurization at RPV failure. Blowdown of the reactor vessel following failure at elevated pressure contributes directly to containment pressurization. High RPV pressures promote entrainment of the debris from the lower drywell and debris fragmentation.

Subsection 19EA.3.1 describes the mechanism for entrainment and the potential for debris dispersal in the ABWR.

Two pressure regimes are considered:

High > 1.37 MPa

Low  $\leq$  1.37 MPa

For sequences with low RPV pressure at the time of vessel failure, the mechanisms which may lead to rapid containment pressurization are generally not operative. As discussed in Subsection 19EA.3.1, entrainment of the debris is an essential prerequisite for DCH. The entrainment of debris from the lower drywell occurs due to levitation by the steam expelled from the vessel after vessel failure. For sequences with the RPV at low pressure at the time of vessel failure, there is no driving force for the steam. Consequently, in the event tree for early containment failure due to DCH, the probability for early containment failure for low-pressure sequences is set to zero.

For high-pressure sequences, on the other hand, mechanisms such as DCH and RPV blowdown may challenge the integrity of the containment. The remaining events on the event tree assess those mechanisms which impact containment loading for high-pressure sequences.

This event is quantified based on the sequence accident class. This is a sorting type event. The probability of each branch is either 0 or 1 depending upon the attributes of the accident class.

#### **19EA.2.1.3 Mode of RPV Failure (MODRVFAIL)**

Following slumping of the molten core debris into the lower RPV head, thermal attack on the lower head and lower head penetrations will eventually result in bottom head failure (unless the debris is cooled in-vessel). Several modes of vessel failure have been considered to be possible ranging from a limited area failure of one or more instrument tubes, drains or control rod drives to creep-rupture failure of the lower head resulting in a large diameter failure.

This event is a split fraction, representing uncertainties in the phenomenology. Two size classes were defined for this study:

Small: Initial area equal to the area of one control rod drive penetration  
( $< 0.1 \text{ m}^2$ )

Large: Nominal failure area of  $2.0 \text{ m}^2$

For quantifying this event, the results from NUREG/CR-4551 were used as guidance. In this analysis, as in NUREG/CR-4551, it was assumed that all breach sizes greater than  $2.0 \text{ m}^2$  could be treated identically. For all core damage sequences where core damage progression is not terminated in-vessel (and vessel failure is predicted) NUREG/CR-4551 indicated that the mean probability of small penetration failures was 0.75 and the probability of large lower-head failure modes was 0.25.

Analyses performed subsequent to NUREG/CR-4551 indicate that the probability of large creep-rupture lower-head failure modes may have been overestimated (References 19EA-3 and 19EA-4). Even though the best-estimate studies indicate a small penetration failure is expected, this analysis addresses hole sizes up to  $2.0 \text{ m}^2$ . The probability of a larger failure is judged to

be quite low based on References 19EA-3 and 19EA-4. Therefore, the probability of large lower-head failure modes has been decreased in this analysis.

The probabilities are considered to be appropriate for both early and late core damage sequences. Vessel ablation is primarily controlled by the superheat in the core debris, and is less influenced by the time of core damage. Thus, the time of core damage will have little effect on the mode of vessel failure.

#### **19EA.2.1.4 Fraction of Core Inventory Molten in Lower RPV Head (RVCORMASS)**

This parameter largely defines the potential for large scale DCH events. It is generally considered that only the debris that is molten in the lower head at the time of vessel breach will have the potential for dispersal and fragmentation. Thus, only this material can significantly contribute to DCH.

Two regimes are considered:

Small	0–20% Core Debris Inventory (Nominal 10%)
Large	20–60% Core Debris Inventory (Nominal 40%)

These mass regimes are similar to those chosen in NUREG/CR-4551 to represent the Grand Gulf plant.

NUREG/CR-4551 provides probabilities for three cases which also appear to be applicable to the ABWR. The mean NUREG/CR-4551 probabilities are presented below:

(1) Case 1

For sequences with water injection into the reactor vessel prior to vessel breach by low-pressure or high-pressure injection systems:

$$P(\text{Small}) = 0.975$$

$$P(\text{Large}) = 0.025$$

(2) Cases 2 and 3

For high- and low-pressure sequences without in-vessel injection:

$$P(\text{Small}) = 0.9$$

$$P(\text{Large}) = 0.1$$

Since the majority of ABWR core damage sequences do not involve late water addition to the core, it is conservatively assumed that the Case 2/3 results apply to all ABWR core damage sequences.

It can be shown that the core debris discharge rates used in the ABWR DCH analysis bound results typical of a BWRSAR calculation (Reference 19EA-5). Table 19EA-2 compares the approximate debris masses participating in DCH at selected intervals after the vessel has failed. The ABWR DCH analysis column shows the values used for a *small* mass of molten debris in the lower head at RPV failure. It should be noted that debris entrainment will occur only until the vessel has depressurized to about 1.379 MPa (200 psia). The BWRSAR results indicate that the RPV depressurizes in about four minutes. The analysis of this study has a much larger vessel failure area due to ablation, thus, the depressurization is more rapid. The pressurization of the containment is most rapid before the wetwell connecting vents clear. Vent clearing will occur within the first second of the blowdown. Therefore, the very early stages of the debris pour and entrainment are the most significant.

The total mass of debris and the zirconium mass used in this analysis are much larger than the masses calculated by BWRSAR. Indeed, the mass of the zirconium bounds the entire zirconium and metal mass calculated by BWRSAR for the critical, early stages of the blowdown. Since the heat of reaction for the oxidation of zirconium is much higher than that of other metals, the use of a high zirconium mass bounds the effects of the other metals. Even at the four minute mark, the distribution of the masses is conservative due to the relative heats of reaction for zirconium and other metals. Thus, the table clearly shows that the assumed masses bound the BWRSAR results.

#### **19EA.2.1.5 High-Pressure Melt Ejection (HPME)**

For sequences with high RPV pressure at vessel failure, the core debris is likely to be expelled from the vessel at high velocity. Furthermore, the velocity of the residual gases blowing down from the reactor vessel are likely to be sufficiently high to result in significant entrainment of the debris from the lower drywell and to result in dispersal and fragmentation of the debris. This event is a split fraction indicating the uncertainty in phenomena. The question evaluates whether a substantial fraction of the core debris is expelled from the vessel at high velocity and followed by the blowdown of the vessel. Given these precursors, it is believed that material will be lifted from the lower drywell floor. A subsequent event heading (FRAG) will assess the extent of debris fragmentation, and dispersal into the upper drywell.

For all cases where reactor vessel failure occurred under high-pressure conditions, the probability of an HPME was assessed to be 0.8 for the Grand Gulf plant in the NUREG/CR-4550 study. Based on similarities in the design of the ABWR and BWR-6 vessel bottom heads, it is assumed that these results can also be applied to the ABWR. Additional discussion is provided in Subsection 19EA.3.1. The “No HPME” value of 0.2 represents the potential that the gas from the RPV will break through the core debris and the vessel will be depressurized prior to the release of the core debris and the potential that the initial vessel breach will be near

the melt surface. BWRSAR results (Reference 19EA-5) indicate that the RPV depressurizes before any substantial amount of core material is expelled from the vessel.

For reasons similar to those discussed above for low-pressure sequences, if an HPME event does not occur, then the loads imposed on the containment structure at vessel failure will not result in a serious threat to containment integrity and the probability of early containment failure is assumed to be zero.

#### **19EA.2.1.6 Fraction of Entrained Debris Fragmented and Transported to the Upper Drywell (FRAG)**

This branch in the DETs is a split fraction event. For high-pressure sequences where an HPME has occurred, this event assesses the extent of dispersal and fragmentation of the entrained debris. In order for a serious overpressure challenge of the containment by direct containment heating (DCH) to occur, a significant fraction of the debris that was molten in the lower RPV head at vessel failure must be transported from the lower drywell into the upper drywell and fragmented. The mechanisms which may limit the transport of the molten debris from the lower cavity to the upper cavity are discussed below. These include:

- (1) Trapping of the debris in the lower drywell.
- (2) Impaction and removal of the debris in the gas transport pathway connecting the lower and upper drywell compartments.
- (3) Partitioning of the gas (and entrained debris) flow exiting the lower drywell between the upper drywell and the wetwell.
- (4) Debris dispersal by wave formation rather than by small particles.

The above mechanisms can impact the extent of debris dispersal to the upper drywell as small debris particles which is the critical parameter for determining the potential threat from DCH.

The basic configuration of the ABWR lower drywell is shown in Figure 19EA-7. Additional details can be seen in the arrangement elevation drawing (Figures 1.2-2 and 1.2-2a), the lower drywell elevation (Figures 1.2-3b and 1.2-3c) and the arrangement plan (Figures 1.2-13e through 1.2-13h). The vessel skirt of the ABWR is solid, there are no openings in it which could connect the upper drywell to the lower drywell. This precludes water transport from the upper drywell into the lower drywell following a LOCA. Hence, the flow path for gases and debris expelled from the lower drywell will be through the downcomers. The upper drywell to wetwell downcomers are imbedded in the lower drywell wall. The downcomers are also connected to the lower drywell gas space via horizontal pipes which penetrate the lower drywell wall at an elevation approximately two-thirds of the height between the lower drywell floor and the top of the lower drywell.

Because of the lower drywell configuration, it is expected that some fraction of the molten debris which is released at vessel failure will be trapped in the lower drywell. The region of the lower drywell above the downcomers does not have any open flow paths. Furthermore, the control rod drive mechanisms are located in this region. Therefore, the velocities in this region will be lower than that in the region below the downcomers. Material which has been lifted off the floor could become trapped in these more stagnant regions of the lower drywell above the downcomer. Thus, one would not expect that all of the debris entrained in the gas flow would exit the lower drywell.

Once debris is assumed to leave the lower drywell and enter the downcomer, two mechanisms govern the final distribution of core material. These mechanisms are the impaction of core debris on structures and the transport to the suppression pool due to flow toward the wetwell in the downcomer. The gas transport pathway to the upper drywell is relatively convoluted. For the debris to enter the upper drywell, it must be entrained off the drywell floor, flowing vertically along the drywell wall. It then turns 90 degrees to enter the horizontal piping. After flowing a short distance through the horizontal piping, the flow will encounter a Tee type junction with the vertical downcomer. At this point the entrained debris must again turn 90 degrees. There is potential for impaction on the downcomer wall at each turn. This impacted debris is likely then to flow downward along the downcomer wall toward the wetwell vents. This effectively removes the material from participating in the DCH event.

In addition, if the horizontal wetwell vents have cleared then the entrained flow will split between that going upward toward the upper drywell and that going downward toward the wetwell vents. If the vents have not (yet) cleared, then all the flow will go upward toward the upper drywell. The debris that partitions with the gas flow going downward toward the wetwell vents will not participate in DCH.

Finally, since DCH relies on the rapid heat transfer from the corium to the surrounding gas, any debris which is transported via a wave type motion will not participate in the DCH event. As discussed above and described in detail in Subsection 19EA.3, wave formation is not expected to be the dominant transport mechanism. Most of the debris transported to the upper drywell is expected to be in the form of particulate.

The fraction of the molten debris in the lower head that is dispersed into the upper drywell and fragmented can be represented by the following relationship:

$$f_{\text{frag}} = f_{\text{downcomer}} \times f_{\text{impact}} \times f_{\text{split-updw}} \times f_{\text{part}} \quad (19\text{EA}-1)$$

where:

$$f_{\text{frag}} = \text{The fraction of debris transported to the upper drywell and fragmented,}$$



- $f_{\text{downcomer}}$  = The fraction of debris which gets entrained out of the lower drywell into the downcomers,
- $f_{\text{impact}}$  = The fraction of the debris entering the downcomers which does not remain permanently impacted on the downcomer walls (i.e. either is not impacted or is impacted and re-entrained),
- $f_{\text{split-updw}}$  = The fraction of the gas flow which goes upward toward the upper drywell (as opposed to the wetwell),
- $f_{\text{part}}$  = The fraction of the debris entrained into the upper drywell which enters in the form of small particles.

The uncertainty ranges for these four parameters were chosen based on the physical layout of the lower drywell along with engineering judgment. The value chosen to represent the amount of material expelled from the vessel which exits the lower drywell represents the potential for material to be trapped in the stagnant region above the horizontal vent pipes. The ANL experiment described in Subsection 19EA.3.1.2.2 did not include any below vessel structures. It may be possible to freeze and hold material on these massive structures. Furthermore, the openings from the ANL cavity are much wider than the openings in the ABWR. Since the debris will have to make a turn to enter the ABWR openings, the smaller area makes the debris less likely to entrain. Based on the above discussion, about half of the debris is assumed to reach the connecting vents.

The debris leaving the lower drywell will then travel a short distance before entering a tee junction. It is expected that some of the debris will impact on the wall of the pipe at the junction and flow down into the wetwell. Based on the physical characteristics of the debris flow path, it was judged that most of the debris does not get removed due to impaction.

Prior to clearing of the horizontal vents, gas flow into the vent pipes will be directed up into the upper drywell. As the upper and lower drywells pressurize, the water level within the vent pipes will be depressed, and venting into the wetwell will begin. The average vent clearing time is 0.5 seconds. After the vents have cleared, the gas would preferentially flow into the wetwell since the upper drywell would be increasing in pressure. If the wetwell and upper drywell pressures were conservatively assumed to be equal, then a 50/50 split would occur based on equal flow areas in both directions. As described in Subsection 19EA.3, the entrainment dispersal time is estimated to be two seconds. If the debris is dispersed linearly, then the vents would clear after only 25% of the debris was released from the lower drywell. The debris leaving the lower drywell after vent clearing would then conservatively be split 50/50 between the wetwell and the upper drywell. Based on this discussion, it was conservatively assumed that most of the debris flows to the upper drywell.

The final phenomenon that could influence the amount of the debris that would participate in DCH is the wave formation. If the debris enters the upper drywell in the form of a coherent wave, it would not be expected to participate in mixing with the gas. Experiments performed at ANL for PWR cavity configurations have resulted in this wave type of sweepout. As discussed in Subsection 19EA.3, wave formation is not expected to be the dominant removal mechanism for the ABWR configuration. However, as debris flows through the wetwell/drywell connecting vents to the upper drywell, it is possible that some of the debris forms wave-like sheets. Therefore, engineering judgment has been used to estimate that the median value for the fraction of debris that is dispersed as particulate debris is 0.875.

Assuming a uniform distribution for each of these parameters between their assessed upper and lower bounds, the distribution for  $f_{\text{frag}}$  was evaluated.

Based on the above discussion, three regimes were selected to represent this parameter in the event tree:

- Low ( $f_{\text{frag}} \leq 0.35$ ),
- Intermediate ( $0.35 < f_{\text{frag}} \leq 0.60$ ), and
- High ( $f_{\text{frag}} > 0.60$ ).

In the deterministic DCH pressure calculations described in Subsection 19EA.3, the nominal values for  $f_{\text{frag}}$  used to represent these three regimes were 0.25, 0.5, and 0.75.

#### 19EA.2.1.7 Peak Containment Pressure Following RPV Failure

This event assesses the peak drywell pressure following RPV failure. There is only one branch for this event. This event summarizes the deterministically calculated drywell pressure for the set of conditions and assumptions specified in the event sequence pathway leading to this event. A description of the calculational methodology and calculated results are presented in Subsection 19EA.3.

#### 19EA.2.1.8 Drywell Head Fails Following Vessel Failure

This event assess the probability of drywell head failure given the pressure determined in the previous event. The probabilities for failure are determined from the drywell head fragility curve described in Attachment 19FA.

### 19EA.3 Deterministic Model for DCH

A computer program has been developed to provide scoping calculations for DCH events in the ABWR. Several simplifications and assumptions exist in this model. This model, and its application to the ABWR design are described below.

**19EA.3.1 Debris Dispersal in the ABWR**

The purpose of this subsection is to briefly summarize the available information on debris dispersal from a configuration like that of the ABWR lower drywell.

**19EA.3.1.1 Velocity Required to Transport Debris Particles**

The velocity required to transport debris particles out of a compartment by entrainment can be easily estimated (Reference 19EA-6). To lift a particle of radius  $r$  against the force of gravity requires a velocity given by:

$$(\rho_f - \rho_g) \frac{4}{3} \pi r^3 g = c_d \pi r^2 \frac{\rho_g u_g^2}{2} \quad (19EA-2)$$

where:

$\rho_f$	=	Fluid density
$\rho_g$	=	Gas density
$r$	=	Particle radius
$g$	=	Acceleration of gravity
$c_d$	=	Drag coefficient
$u_g$	=	Gas velocity

If we assume complete hydrodynamic breakup, the maximum particle radius is given by equating the force imparted by the gas stream to the surface tension force holding the droplet together. This is usually cast in terms of a Weber number:

$$We = \frac{2c_d \rho_g u_g^2 r}{\sigma} \quad (19EA-3)$$

where:

$\sigma$	=	Surface tension
----------	---	-----------------

There is some ambiguity on the form of this equation and the choice of the Weber number,  $We$ . Most authors fold the drag coefficient into  $We$ . This coefficient is explicitly left in the expression. Typical values of Weber number are 6 to 12 when the drag coefficient is left out. Strictly speaking, these would specify the maximum particle size. The mass median diameter, for example, would be about half this value (Reference 19EA-8).

If we substitute Equation 19EA-3 into 19EA-2 and neglect the gas density compared to the liquid density, we obtain:

$$u_g^4 = \left( \frac{4We}{3c_d^2} \right) \frac{\rho_f \sigma g}{\rho_g^2} \quad (19EA-4)$$

Define the Kutateladze number by:

$$Ku = \frac{u_g}{\left( \frac{\rho_f \sigma g}{\rho_g^2} \right)^{1/4}} \quad (19EA-5)$$

so that:

$$Ku = \left( \frac{4We}{3c_d^2} \right)^{1/4} \quad (19EA-6)$$

A free particle in the high Reynolds number limit has a drag coefficient of about 0.44. If we assume a Weber number of 8 (the results obviously depend weakly on this choice), we obtain:

$$Ku = 2.7 \quad (19EA-7)$$

When substituted into Equation 19EA-5, this gives a velocity close to the experimentally measured value required to entrain particles off a free surface (Reference 19EA-9).

Consider a different situation in which gas is sparging a pool from below. If we consult Figure 19EA-10 (Reference 19EA-6) which shows the drag coefficient for various porosities ( $\epsilon$ ), we note that the drag coefficient for a particle bed is in the range 20–80. If we use 80 and leave the We number at 8, we obtain:

$$Ku = 0.2 \quad (19EA-8)$$

This does yield just the experimentally measured velocity required to fluidize a pool (Reference 19EA-10).

Thus, we see that the velocity required to lift liquid droplets is a strong function of the configuration. A gas stream passing horizontally over a liquid pool requires on the order of 10 times the velocity required to fluidize a bed (i.e., a situation in which the gas stream proceeds vertically from below). This effect results from the different drag coefficients which apply to

the two situations. Thus, one would expect the required velocity for entrainment in the ABWR to be 10% of the value for the Zion cavity.

### **19EA.3.1.2 Argonne Experiments on Debris Dispersal**

Spencer, et. al., at Argonne National Laboratory have conducted a number of debris dispersal experiments in several geometries. Extensive information on these is available (References 19EA-10, 19EA-11, 19EA-12, and 19EA-13). Here we shall briefly summarize the results of two sets of quasi-steady experiments designed to determine the threshold velocities required to transport debris from simulated reactor cavity/pedestal regions.

#### **19EA.3.1.2.1 Experiment on Zion Configuration**

Figure 19EA-11 shows a schematic view of the Zion reactor cavity. Experiments conducted with this geometry (Reference 19EA-11) indicate that the threshold velocity required to disperse liquid droplets into the gas stream and move them from the cavity is approximately given by a Kutateladze number of 2.5. This is not unexpected, since the geometry of the cavity is such as to cause the gas jet leaving the reactor to stagnate at the floor of the cavity, to turn and proceed horizontally down the cavity keyway over the liquid pool. Thus, the considerations which lead to Equation 19EA-7 would seem to apply.

It should be noted that sweepout, in which a continuous liquid film was observed to be flooded from the reactor cavity, occurred at about the same velocity as entrainment of droplets. Thus, as noted in Reference 19EA-14, the amount of material transported from a Zion-like cavity as droplets relative to the amount transported as a film is determined by the relative rates of the two processes.

An additional experiment was run in which steel shot of diameter  $780 \times 10^{-6}$  m was used instead of a liquid pool. By substituting into Equation 19EA-2, the drag coefficient necessary to explain the observed velocity threshold for debris dispersal of  $\sim 16$  m/s (Reference 19EA-13) is found to be about 0.3. It is not known why this is less than the expected value of 0.44, but the discrepancy is not considered large.

#### **19EA.3.1.2.2 Experiments on Grand Gulf Configuration**

Figure 19EA-12 shows a schematic view of the Grand Gulf pedestal region. Experiments were also conducted at Argonne on a scale model of this configuration. Quite different behavior was observed in these tests. Due to the more or less symmetric orientation of the scale model CRD ports around the circumference of the pedestal, the gas jet leaving the simulated reactor vessel was observed to stagnate, proceed horizontally so as to undercut the entire liquid pool, turn and proceed vertically using virtually the entire cross-sectional area of the pedestal. (Only a small fraction of the area was used by the jet moving downward from the simulated vessel.)

As noted in Reference 19EA-10, this configuration is reminiscent of a pool sparged from below. Using this reasoning, Equation 19EA-8 would be expected to apply. Indeed, a

Kutateladze number of 0.2 was found to accurately predict the velocity required to initiate removal of debris. Visual observations of the experiment support this conclusion, as it was seen that the entire pool became fluidized, the liquid rose up to the level of the ports, and was then swept out by the gas stream.

An experiment was also conducted in this geometry with steel shot. A drag coefficient of about 7 is required to explain the measured velocity threshold for sweepout of ~3.5 m/s. By consulting Figure 19EA-10, we see that such a drag coefficient is appropriate for a bed of porosity about 0.8. This is, in fact, the porosity that would be obtained if the entire bed of shot was uniformly fluidized up to the elevation of the CRD ports. This suggests that the threshold velocity for sweepout in the Grand Gulf configuration might be a function of the ratio of the initial pool volume to the total volume which exists in the pedestal under the elevation of the gas flow paths. In other words, fluidization could begin at a low velocity (when the porosity is low and the drag coefficient is high), but as the pool tries to grow toward the exit flowpaths, the velocity required to continue to levitate droplets would increase. This conjecture cannot be confirmed by the few tests run with liquid pools, however.

#### **19EA.3.1.2.3 Application to ABWR Configuration**

The ABWR configuration, Figure 19EA-7, is similar to that for Grand Gulf. Thus, we expect that a Kutateladze number on the order of 0.2 should be applied to calculate the dispersal threshold. With the exception of the ANL Grand Gulf work, the documented experiments performed to date have focused on PWR type cavities such as Zion. As discussed above, these are not directly applicable to the ABWR configuration.

#### **19EA.3.2 Pressurization Due to DCH**

The pressurization of the drywell is affected by the blowdown of gases from the vessel and by the heat transfer from fragmented corium into the drywell. An explicit method is used to calculate the response of the system. The gas is assumed to be an ideal gas with the rate of change of pressure,  $\dot{P}$ , calculated from:

$$\dot{P} = \frac{M_g R T_g}{MW_g V} + \frac{\dot{M}_g R T_g}{MW_g V} \quad (19EA-9)$$

where:

$M_g$  = Total mass of gas in containment (steam and non-condensable gas)

$R$  = Gas constant (8314 N•m/kg•mole•K)

$T_g$  = Gas temperature

$MW_g$  = Average molecular weight of the gas mixture

$\dot{V}$  = Drywell volume

and a dot over a variable indicates its rate of change with time.

The temperature change of the gas,  $\dot{T}_g$ , is calculated by assuming that the gas and the fragmented debris are in equilibrium at each time step. Since the DCH event is very rapid, no credit is taken for heat transfer to containment heat sinks. The specific heat capacity for steam is evaluated using a curve fit to saturated steam properties (Reference 19EA-15). Constant specific heat is used for the non-condensable gas.

The rate of change of mass in the containment,  $\dot{M}_g$ , considers the gas blowdown from the vessel, any flow to the suppression pool through the connecting vents, and hydrogen generation which occurs as a result of the reaction between the steam and the zirconium. The mass flow rates through the downcomers and from the vessel are evaluated using a compressible flow model (Reference 19EA-15). The pressurization of the wetwell due to any addition of non-condensable gases is considered. Steam which passes through the connecting vents is assumed to be quenched.

The debris conditions are calculated by conservation of energy in the system. The mass of debris participating in the DCH event is assumed to increase linearly over the time constant for the event (discussed in Subsection 19EA.3.4). The fraction of the debris allowed to oxidize is a user input (discussed in Subsection 19EA.3.5). The energy of reaction is taken to be that for the zirconium steam reaction. Oxidation of the zirconium participating in the DCH event is assumed to be instantaneous.

The temperature of the debris is calculated based on the amount of energy remaining with the phase change energy accounted for and assumed to take place at a uniform temperature of 2500 K. Constant specific heat and latent heat of fusion are assumed.

### **19EA.3.3 Calculation of Vent Clearing Time**

The DCH program previously described includes a model to predict the time required to clear the horizontal vents and begin gas flow to the wetwell. The model, based on analysis by Moody (Reference 19EA-16), requires as input the pressurization rate for the upper drywell. The DCH model computes the pressurization rate for each time step. Given this, Moody has derived a simple formula for the water velocity resulting from this ramp pressure. The DCH model then computes the water movement as a function of time; and, based on a table look up of vent area vs. water level, calculates the appropriate drywell vent area at any point in time.

### **19EA.3.4 Calculation of Dispersal Time Constant**

For the parametric modeling of DCH in this analysis, a timescale for dispersal must be input. This influences the rate of containment pressurization by defining the entrainment rate of the debris.

There is a dearth of good models for DCH. The only models which were identified are:

(1) The CONTAIN Model

This is a lumped parameter model in which the rate of entrainment is input by the user. It provides no insights for this study.

(2) Henry has developed a model for ARSAP (Reference 19EA-17) that explicitly compares the time-scale for dispersal due to the acceleration of the liquid film as a whole to the time required to entrain the debris as droplets.

This model is very attractive from the standpoint that it produces closed-form answers and illustrates that the competition between the two modes of debris removal from the cavity may be an important consideration for designing and interpreting experiments. However, there appear to be several problems with this model. First, it assumes a very schematic debris configuration, i.e. an initially static debris pool lying on the floor of the cavity. It seems more reasonable to assume that there is debris splashing throughout the cavity, as point out in Levy's WRSIM papers (Reference 19EA-18) and in Spencer's work at ANL. Next, it is questionable that the entrainment rate formula that is used, the one developed by Ricou and Spalding for gas-gas entrainment, applies to this situation. There is evidence (cited by Levy) that non-uniform gas velocities in cavities may play an important role in enhancing entrainment rate. Finally, only very limited comparisons to data have been offered.

Taken at face value, Henry's model tends to predict very rapid removal of the debris from the cavity, mainly as a liquid film. Oddly enough, the time-scale for removal of the film depends only in a very weak way on the hole size in the vessel (i.e. through the gas density in the cavity and even this matters only as the 0.25 power).

(3) BNL has written a one-dimensional model called DCHVIM. In a summary paper presented at the Pittsburgh Heat Transfer conference in 1987, the model is applied to the SNL DCH-1 experiment. For this calculation, however, the entrainment rate was taken directly from experimental data. In addition, the model was not applied to a full, reactor-scale scenario, only to DCH-1.

(4) Sienicki and Spencer at ANL have written a relatively sophisticated one-dimensional hydrodynamics model called HARDCORE (Sienicki and Spencer, undated). Separate mass, momentum and energy equations are written for the liquid film, the droplets and the gas. The entrainment correlation is based on liquid jet breakup formulas developed by De Jarlais, Ishii, and Linehan. Being one-dimensional, the model does not, of course, taken into account non-uniformities in velocity, though there is consideration given to entrainment from annular films on the cavity walls.



The model was applied to the ANL CWTI-13 experiment and to DCH-1. In both cases, it is stated that the debris entrainment time was predicted fairly accurately by the code (time-scales on the order of 0.1 seconds). When the code was then applied to a full-scale Zion TMLB accident, the predicted time-scale for sweep-out of the debris from the cavity was of order 2.5 seconds, i.e. the numerical results are fit rather well by:

$$m_e = m_o(1 - e^{-t/2.5}) \quad (19EA-10)$$

where:

$t$  = Time in seconds since the blowdown begins

$m_e$  = mass entrained

$m_o$  = initial mass available for entrainment

- (5) The recent papers by Levy, mentioned above, contain an explicit closed-form expression for the time-dependent entrainment of debris from the reactor cavity. This formula has been compared to a wide variety of small-scale test data with remarkably good results. The formula was applied to calculate the entrainment rate for a full-scale Zion-like cavity in a TMLB-type sequence. If one assumes that steam exists in the cavity (the results are apparently quite sensitive to the gas density there due to the strong dependence on Euler number), one obtains the seemingly nonsensical result of 100 seconds. However, it does not appear at this juncture that a constant in his expression can be derived from small-scale experiments and applied to full-scale cavities as was done in the calculation just mentioned.
- (6) A code called CORDE is under development in the UK. We have very little information on its models, state of development, or predictions.

Thus, based solely on the ANL paper, the assumption used in this analysis is linear debris removal assumed over a 2-second period. This value appears to be conservative, but not remarkably so. Figure 19EA-13 compares the fraction of debris discharged for the 2-second linear rate used in this analysis with the 2.5-second e-folding time from the ANL study. The sensitivity to this assumption is investigated in Subsection 19EA.3.6.

### **19EA.3.5 Application of DCH Model to ABWR**

The model requires a variety of inputs which describe the geometry of the vessel and containment, the initial and boundary conditions for the event and a few model parameters.

The geometric information required by the model is:

- (1) The drywell vessel and wetwell gas free volumes which are used to calculate pressure.

The drywell volume used for this analysis is the total for the ABWR upper and lower drywells. This effectively assumes that there is a large flow area between upper and lower drywell regions. The possible impact on the results from this assumption is considered in Subsection 19EA.3.6.4.

- (2) A table of horizontal vent area as a function of distance from the initial water level and the total vent clearing depth when all vents are available.

These are used to calculate the vent clearing time. For this analysis, it is assumed that there is no initial pressure difference between the wetwell and the drywell. Thus, water level in the connecting vents is high, which conservatively delays the time until the vents begin to uncover and gas can flow to the wetwell.

- (3) The vessel failure area which is used to calculate the blowdown from the vessel.

This value is specified for each branch point on the DETs.

Initial and boundary conditions are:

- (1) Debris Mass Involved in DCH Event.

The value of this variable is specified for each case on the DETs.

- (2) Initial Debris Temperature.

If this temperature is specified above 2500 K, then the latent heat of fusion is used in calculating the initial debris energy. If the temperature is at 2500 K or below, then the latent heat of fusion is not included in the initial debris energy. This value was nominally set at 2501 K. The sensitivity to this assumptions is investigated in Subsection 19EA.3.6.3.

- (3) The initial containment temperature and pressure are assumed equal in the wetwell and drywell.

The steam mass fraction in the drywell is assumed to be 1.0. The sensitivity to this assumption is investigated in Subsection 19EA.3.6.6.

- (4) The initial vessel pressure is used to calculate the source of steam from the vessel to the containment volume.

The pressure is assumed to be the nominal vessel pressure for normal operating conditions. Slight variations in this value (such as might result from a consideration of the SRV setpoints) do not have a significant impact on the results. No attempt is taken in this analysis to take credit for partially depressurized vessel conditions.

- (5) Vessel gas temperature and vessel steam enthalpy.

Both values are conservatively taken to be constant. The values used are typical for MAAP analyses of high-pressure core melt scenarios.

Model parameters are:

- (1) Fraction of Zr to be Oxidized in The DCH Event.

Of the debris mass that is being entrained at any instant, 20% is assumed to be Zr. This debris is assumed to oxidize immediately as it is entrained. Therefore, if one specifies 0.5 as the oxidation fraction, then half of that 20% mass will oxidize. For every mole of Zr, 2 moles of H<sub>2</sub>O will be replaced by 2 moles of H<sub>2</sub> in the drywell volume, and the chemical reaction energy will be added to the debris. The sensitivity to this parameter is discussed in Subsection 19EA.3.6.5.

- (2) The time for debris entrainment determines the interval during which the specified mass of debris will be entrained.

Refer to Subsection 19EA.3.4 for a discussion of this parameter. The sensitivity to this parameter is investigated in Subsection 19EA.3.6.2.

- (3) Time Constant for DCH.

If set to zero, the debris will be entrained linearly. If set to non-zero value, then the debris will entrain at a rate with an e-fold value equal to the time constant. This analysis assumes the debris is entrained linearly. Any sensitivity to this parameter is bounded by the time for debris entrainment sensitivity discussed in Subsection 19EA.3.6.2.

- (4) The time step for the computer code calculations was selected to be one millisecond.

Since the time constant for the DCH event is on the order of a few seconds, there should be no sensitivity to reasonable variations in this parameter.

The DET methodology addresses the variation in debris mass, initial containment pressure, and vessel failure area. Subsection 19EA.3.6 provides a discussion of the importance of the debris temperature, Zr fraction, dispersal rate, nodalization and initial drywell steam fraction.

The code calculates the containment response to DCH events. The most important output of the calculation is the peak containment pressure. The results of the model analysis for each branch of the DETs are summarized in the penultimate column of Figures 19EA-4, 19EA-5, and 19EA-6.

### **19EA.3.6 Sensitivity to Various DCH Parameters**

As indicated in Subsection 19EA.2, the DET methodology addresses the variation of several key DCH parameters. This subsection looks at the importance of the debris temperature, amount of Zr oxidized ex-vessel, and the dispersal time constant to the overall pressurization. These parameters were assumed to be constant in the scoping calculations and were judged not to have a significant impact on the results. The results of the sensitivity studies confirm that these parameters have a second order effect on the peak containment pressure.

#### **19EA.3.6.1 Base Case**

For the purpose of comparison, the following case was analyzed using the DCH model:

- (1) Fraction of core molten at vessel failure—40%.
- (2) Fraction of material dispersed into the upper drywell—50%.
- (3) Dispersal time—2 seconds.
- (4) Initial containment pressure—1.5 atmosphere.

The result of the analysis indicates a peak drywell pressure of 0.903 MPa. Referring to the containment failure curve, this has a failure probability of about 0.17.

#### **19EA.3.6.2 Dispersal Time**

The base case was re-run assuming dispersal times of 1 and 3 seconds. The results are:

	<b>Peak Drywell Pressure</b>
	<b>MPa</b>
Base Case	0.903
Dispersal Time = 1	1.124
Dispersal Time = 3	0.758

Subsection 19EA.3.4 provides the justification for the 2-second dispersal time and indicates that it may be somewhat conservative. However, a 50% increase in the dispersal time resulted

in only a 20% change in the peak containment pressure. This does not represent a very significant change.

Subsequent to the completion of the DCH analysis, Ishii (Reference 19EA-19, Section 3.4.1) developed a model for the calculation of a removal time constant. Ishii's model assumes that droplets are stripped off a film adhering to the walls as compared to the ABWR model of a "sparged pool" to calculate whether gas velocities are high enough to cause debris removal from the lower drywell

To apply the analysis to the ABWR, Ishii's calculations were first duplicated. This proved to be somewhat difficult, because a few of the key physical and geometrical parameters are not supplied in the reference. By using debris property values from the literature and back-calculating some of the geometrical parameters from intermediate results, we obtained a consistent set of parameters that resulted in agreement within about 10 percent on the various results of interest.

If one first assumes the same vessel breach diameter as in the Ishii's calculation (0.2 meter diameter, which is a typical value for an ablated localized failure given the debris masses and temperatures likely to exist), one finds that the flow out of the lower drywell in ABWR never becomes choked. The area-averaged velocity in the lower drywell is an order of magnitude too small to meet the Ishii-Grolmes entrainment criterion.

This is the same result we obtained in the PRA for the low breach area limit. In the PRA, we concluded that it would be appropriate in the interests of conservatism to use Spencer's Mark III results to predict the potential for debris removal from the lower drywell. The original analysis we made of Spencer's experiments recognized that the volume which exists below the pedestal vents could be large compared to the debris volume. Therefore it is not clear that the sparged pool mechanism can always function in a Mark III-like configuration to remove the debris at velocities much lower than the droplet stripping mechanism. As it turns out, the volume beneath the vents in ABWR is very large ( $\sim 100 \text{ m}^3$ ) compared to the debris volume ( $5\text{-}10 \text{ m}^3$ ).

To illustrate, consider the situation as the two phase debris pool level tries to approach the height necessary for debris entry into the connecting vents. This requires such a large pool void fraction in ABWR (e.g.  $> 90\%$  if the pool is uniformly swelled) that the drag coefficient based on the superficial velocity will drop to values approaching that for isolated drops. In the limit, one merely regains the  $Ku \sim 3$  result that is used in typical PWR geometries. This suggests that very little debris could be removed from the ABWR lower drywell, which is, of course, a far more favorable result.

A possible alternate mechanism for getting the debris to the connecting vents is to imagine that the inertia of the debris film (or perhaps the inertia of the droplets which are created during the sparging process) carries debris to the vicinity of the connecting vents. The higher gas velocities in the vicinity of the connecting vents would then tend to draw debris into the vents.

Considering that the vents are located 10 meters above the floor and that they occupy only about a third of the perimeter at that elevation, this does not seem to be a very effective mechanism either. One could also cite the observations in the Sizewell experiments (Reference 19EA-19, Appendix O) of very high gas velocities near the floor of the cavity and speculate that this might apply near the drywell wall surface. All in all, however, it appears that there is very little likelihood of entrainment in the ABWR PRA for cases with localized vessel failures.

Nevertheless, if one postulates that the debris does make it into the connecting vents by some mechanism, one can then apply Professor Ishii's analysis. At one atmosphere (the pressure used in the Ishii's calculation), the velocities in the pipe are slightly less than the entrainment threshold ( $\sim 80$  m/s) calculated by the Ishii-Grolmes model. The analysis proceeds in a straightforward manner except that it is difficult to estimate the debris film velocity and typical thickness without postulating the mechanism that got the debris to the vents in the first place (this actually presents problems in Ishii's PWR analysis as well). If one uses the Ishii's technique, these quantities are estimated using

$$u_f \delta_{typ} = \frac{A_j u_j}{\pi D_h} \quad (19EA-11)$$

where  $j$  denotes conditions in the jet leaving the vessel and  $D_h$  is the hydraulic diameter of the lower drywell. One then obtains a total entrainment rate from all the connecting vents of about 1 tonne/s (recall, however, that the entrainment criterion is not quite satisfied). This results in a time constant for debris entrainment on the order of 20-70 seconds, depending on the assumed debris mass, which is much longer than assumed in the PRA.

We now turn our attention to the large end of the vessel breach area spectrum. This was taken to be  $2 \text{ m}^2$  in the PRA and was assigned a conditional probability. In this case, flow from the cavity will be choked. In the Ishii's calculation, the cavity flow area is the same as the area connecting the cavity to the containment. To calculate the gas velocity, the initial cavity pressure and the vessel gas temperature (isothermal blowdown) were used which presumably maximizes the velocity. If one follows the same procedure here a velocity of 230 m/s is obtained at an initial pressure of 2.5 bar. This is much greater than the entrainment velocity of about 70 m/s.

Gas velocities will be higher still in the connecting vents, which have about one tenth the flow area of the drywell. In the light of the previous discussion, it is assumed that the overall process of debris removal from the lower drywell is limited by the entrainment rate in the lower drywell, not the processes of de-entrainment and subsequent re-entrainment in the connecting vents.

The entrainment rate calculated in the lower drywell at 230 m/s is very large, on the order of 1500 tonne/s. It is doubtful that the correlations would be valid under such extreme conditions. Even if the equations do apply, the drywell pressure and gas density would rapidly increase due

to the effect of the rapid transfer of momentum to the debris. This would invalidate the assumptions used in the calculation which maximized gas velocity.

These results supply useful insights. However, the overall impact of these considerations on the results of the PRA are relatively small. The small vessel breach area cases supplied half the conditional failure probability from DCH in the PRA. It appears that the likelihood of DCH-induced failures was overestimated for these cases since it is not at all clear that debris entrainment into the connecting vents can occur. In the large breach area cases, a more refined analysis which took into account the effect of the blowdown and debris entrainment on the thermal-hydraulic conditions in the lower drywell over the period when entrainment was occurring would be necessary to better quantify the likelihood of overpressurizing the lower drywell. For perspective, if all large vessel breach cases were assumed to result in containment failure, the conditional containment failure probability would be small. In any event, it is clear that the chance of significant DCH is determined largely by the assumptions used to characterize the upper extreme of the vessel breach spectrum.

In closing, it is noted that the implications of having a reduced chance of debris transport to the upper drywell in the majority of cases which have a small breach area may be more important for the upper drywell heat-up issue than for DCH. In particular the long term need for the initiation of the ACIWA system in spray mode may have been overestimated.

#### **19EA.3.6.3 Debris Temperature**

The core debris will interact with a variety of structures as it exits the reactor vessel. Thus, it is expected to experience substantial cooling by those structures on its way to the upper drywell. The ABWR DCH analysis conservatively assumed that the core debris entering the upper drywell was completely molten at a temperature of 2501 K. A sensitivity case was run assuming 2601 K for the debris temperature entering the upper drywell. The results indicate a peak containment pressure of 0.917 MPa vs. the base case value of 0.903 MPa.

#### **19EA.3.6.4 Nodalization**

The DCH analysis combines the lower and upper drywell compartments into a single control volume represented by node 1. The second node is set up to represent the wetwell with the suppression pool in the path connecting node 1 to node 2. A sensitivity case was run to investigate local pressurization in the lower drywell compartment. To do this, the volume included in Node 1 was reduced to that of the lower drywell with the vent area equal to the vent flow area from the lower to the upper drywell (11.3 m<sup>2</sup>). Node 2 was used to represent the upper drywell. Since the junction between node 1 and node 2 does not require vent clearing as in the base case analysis, the vent path was assumed already cleared. All of the gas heating was done within the lower drywell compartment. In order to calculate the correct down-stream pressure, zero initial steam was assumed in the drywell compartment. This is necessary because the model assumes that all steam passing from the first node to the second node is condensed, setting the initial steam fraction to zero will correctly account for the increasing upper drywell

pressure. A detailed examination of the results of this sequence indicates the zirconium oxidation reaction is essentially steam limited. Since the zirconium oxidation process consumes most of the steam exiting the vessel, only a small amount of steam will actually enter the second node.

The peak pressure computed for the lower drywell was 0.765 MPa. This indicates that the lower-to-upper drywell vent area is sufficient to preclude any substantial pressure buildup in the lower drywell region.

#### **19EA.3.6.5 Zr Oxidation Ex-Vessel**

The base case assumed that 20% of the core material that was discharged from the vessel was Zr metal. This is based on a uniform distribution of UO<sub>2</sub> and Zr within the lower plenum of the reactor vessel. Of this material 50% of the Zr that was involved in DCH was allowed to oxidize and contribute to the drywell heatup. This is a conservative value since, in the time frame of interest, only the Zr on the surface of the particles would oxidize.

As a sensitivity calculation, the amount of ex-vessel Zr oxidation was doubled. This change in the amount of ex-vessel Zr oxidation is equivalent to assuming that all of the Zr metal in the debris is oxidized. Alternately, this assumption is equivalent to assuming the fraction of core debris exiting the vessel was 40% Zr instead of 20% assumed in the base case. Thus, this sensitivity addresses both any possible non-uniform core material distribution within the lower head and the potential for increased oxidation.

The peak drywell pressure was computed to be 1.034 MPa vs. the base case value of 0.903 MPa. This is a very small effect given a factor of two variation in the amount of Zr oxidized during the DCH event.

#### **19EA.3.6.6 Initial Drywell Steam Fraction**

Since steam passing through the connecting vents will condense, the amount of wetwell pressurization during the DCH event is limited. The base analysis assumed a 100% steam environment in the drywell at the start of the event. To investigate the impact of this parameter on the peak pressure, a case was run assuming the drywell environment is initially 100% nitrogen. The wetwell pressure will be expected to increase faster for this case resulting in a higher drywell pressure. This result indicates that this is true, although the rise in the peak pressure is small. The peak pressure for this scenario is 0.979 MPa, as compared to a peak of 0.903 MPa for the base case. This variation due to initial drywell gas composition does not have a significant impact on the results of this study.

#### **19EA.3.6.7 Hydrogen Combustion**

Technical specifications allow the ABWR to be operated with 4% oxygen in the containment. During a DCH event, the drywell gas temperature may exceed the auto-ignition limit of approximately 811 K (1000°F). Burning of the hydrogen in the containment with this residual



oxygen could result in an increase in energy of the gas. The appropriate reaction energy was added to the existing corium/gas mixture in order to predict an increase in the peak pressure due to hydrogen combustion. No credit was taken for the reduction in moles which would occur as a result of the burn.

The peak containment pressure increased by 0.103 MPa relative to the base case pressure of 0.903 MPa. The same analysis was performed assuming that the initial steam fraction was 0.0 (as compared to the base case assumption of 1.0). For this second case, the peak pressure increased by 0.228 MPa. Since a 50% steam fraction in the containment more accurately represents the actual conditions, the expected increase in peak pressure resulting from the recombination is 0.172 MPa. This is only a 20% change in the peak containment pressure, and does not represent a very significant effect.

#### **19EA.3.6.8 Vent Clearing**

After core debris discharge and before RPV blowdown, it is expected that the containment will begin to pressurize even before debris is dispersed into the upper drywell. A sensitivity study was run assuming that the vents had already cleared prior to debris dispersal. The results show that the peak containment pressure is reduced by 0.221 MPa compared to 0.903 MPa for the base case. This represents a decrease in the peak pressure of about 20%. While this is not very significant, it does provide a measure of the conservatism in the analysis.

### **19EA.4 Summary of Results**

#### **19EA.4.1 Quantification of Decomposition Event Trees**

The quantified decomposition event trees are shown in Figures 19EA-1 through 19EA-6. The relationship between the peak drywell pressure and the cumulative probability distribution are shown in Figure 19EA-14. Note that the probability distribution functions (PDFs) are discrete since the discrete probabilities were assigned in developing the trees. The PDFs provide a measure of certainty that the pressure will not exceed a given value. They are not, however, uncertainty distributions in a statistical sense. Rather, they are based on knowledge of DCH and engineering judgment which characterize the ability to accurately characterize the boundary conditions for the problem.

From a deterministic viewpoint, the best estimate for the peak containment pressure is given by the median value of the PDF. As can be seen by comparing Figures 19FA-1 and 19EA-14, this indicates that the containment would not be expected to fail for any of the initial containment pressures studied. A measure of the uncertainty in this study is found by using the weighted sum (mean) of the probability of drywell failure for each of the branches on the DETs. These weighted values are transferred to the containment event trees for use as the conditional probability of drywell failure for sequences in which the vessel fails at high pressure.

### **19EA.4.2 Impact on Containment Failure Probability**

An inspection of the ABWR accident classes shows that the conditional probability of having high RPV pressure at vessel failure is moderate.

A calculated probability of early containment failure (from direct containment heating), conditional on core damage, is very small.

#### **19EA.4.2.1 Sensitivity of Containment Failure Probability to Assumptions**

In order to demonstrate the robustness of the containment failure probability to the peak pressures calculated in the deterministic DCH analysis, three additional sensitivity calculations were performed. First, the DET was requantified assuming that the peak containment pressure for each of the low initial containment pressure cases was increased by 0.207 MPa. This could represent the possibility of an initial steam fraction of 50% in combination with a hydrogen burn and no credit for partial clearing of the wetwell connecting vents before the DCH event occurs. The resulting conditional containment failure probability for DCH increased slightly.

The second sensitivity case assumed that the containment would be at intermediate pressure for all cases. This represents potential uncertainties in the hydrogen production during the in-vessel portion of the accident. For this case, the containment failure probability due to DCH increases slightly. Although the conditional probability of failure by DCH is higher in this case than in the base analysis, DCH does not pose a significant threat to the CCFP goal of 0.10.

The third sensitivity calculation assumed that the containment would be at the intermediate pressure for all cases and, in addition, that all peak pressures would be increased by 0.207 MPa. The results show that for this conservative case, the conditional containment failure probability for DCH would be increased. Even with these very conservative assumptions, the DCH containment failure probability is far less than the 0.10 goal for CCFP. This demonstrates a large margin for the ABWR containment design to withstand containment challenges.

### **19EA.4.3 Impact on Offsite Dose**

The final measure of the impact of uncertainties in severe accident phenomena is the effect on offsite dose. The CETs are quantified using the weighted sum of the containment failure probability as discussed above. The results of the CETs are then combined with deterministic accident sequence analysis and consequence analysis to determine the dose associated with the spectrum of severe accidents. In order to indicate the possible variation in dose due to uncertainty in DCH phenomena, other values must be selected for the probability of containment failure due to DCH.

Since the probabilities used in developing the DETs are themselves the uncertainties in the phenomena, one cannot determine the classical 5-50-95 confidence limits. However, one can select pressures corresponding to various cumulative certainty of non-exceedance (shown in Figure 19EA-14) and compare these values to the containment fragility curve (developed in

Attachment 19FA) to estimate the probability of drywell failure with varying degrees of certainty. Selecting the 95% value from Figure 19EA-14 and noting that containment failure is not expected at the 50% certainty for peak pressure, one may conclude that for the accident frequencies and certainty levels of interest, DCH has no detectable impact on the offsite dose.

## **19EA.5 Conclusions**

The ABWR has a highly reliable depressurization system which results in a very low probability of a core damage event which leads to vessel failure at high pressure. Nonetheless, an evaluation of the potential risk of direct containment heating leading to containment failure in the ABWR has been performed. This study indicates that the design of the ABWR is highly resistant to damage as a result of a DCH event. This is due primarily to the general configuration of the ABWR lower drywell and connecting vent configuration and area. No modifications to the containment design are suggested as a result of this analysis.

## **19EA.6 References**

- 19EA-1 "Severe Accident Risks: An Assessment for Five U.S. Nuclear Power Plants", NUREG-1150, U.S. Nuclear Regulatory Commission, June 1989.
- 19EA-2 T.D. Brown, et. al., "Evaluation of Severe Accident Risks: Grand Gulf Unit 1", NUREG/CR-4551, Vol. 6 Rev. 1, Part 2, December 1990.
- 19EA-3 J. L. Rempe, "BWR Lower Head Failure Assessment for CSNI Comparison Exercise", EGG-EAST-9609, April 1991.
- 19EA-4 S.A. Hodge and L.J. Ott, "Failure Modes of BWR Reactor Vessel Bottom Head", ORNL/M-1019, Letter Report, May 10, 1989.
- 19EA-5 S.R. Greene, S.A. Hodge, C.R. Hyman, M.L. Tobias, "The Response of BWR Mark II Containment to Station Blackout Severe Accident Sequences", NUREG/CR-5565, ORNL/TM-11548, May 1991.
- 19EA-6 Fauske and Associates, "Key Phenomenological Models for Assessing Non-Explosive Steam Generation Rates", IDCOR Technical Report 14.1B, June 1983.
- 19EA-7 Not Used
- 19EA-8 M. Pilch, et. al., "Acceleration Induced Fragmentation of Liquid Drops", NUREG/CR-2247, USNRC, August 1981 quoted in J. Sienicki and B. Spencer, "A Multifluid and Multiphase Flow and Heat Transfer for the Prediction of Sweepout from a Reactor Cavity", Proc. Fourth Miami Inter. Symposium on Multi-Phase Transport and Particulate Phenomena, Miami Beach, December 15-17, 1986.
- 19EA-9 S. Kutateladze, "Elements of the Hydrodynamics of Gas-Liquid Systems", Fluid Mechanics-Soviet Research, 1, 4, 1972.

- 19EA-10 B. Spencer, S. Baronowsky, and D. Kilsdonk, "Hydrodynamic Sweepout Thresholds in BWR Mark III Reactor Cavity Interactions", ANL/LWR/SAF-84-1, April 1984.
- 19EA-11 B. Spencer, et. al., "Sweepout Thresholds in Reactor Cavity Interactions", ANL/LWR/SAF 82-1, April 1982.
- 19EA-12 B. Spencer, D. Kilsdonk, and J. Sienicki, "Hydrodynamics Aspects of Ex-Vessel Debris Dispersal in Zion-Type Containment Designs", ANL/LWR/SAF 83-1.
- 19EA-13 B. Spencer, D. Kilsdonk, J. Sienicki, and G.R. Thomas, "Phenomenological Investigation of Cavity Interactions Following Postulated Vessel Meltthrough", Proc. Inter. Meeting on Thermal Nuclear Reactor Safety, NUREG/CP-0027, Volume 2, Session 16, pp. 923-937, Chicago, August 1982.
- 19EA-14 R.E. Henry, "Fission Product Release During High-Pressure Melt Ejection", Task 3.4.6 Report, Advanced Reactor Severe Accident Program, November 1988.
- 19EA-15 "MAAP 3.0 B Computer Code Manual", EPRI NP-7071-CCML, Volume 2, November 1990.
- 19EA-16 Frederick Moody, "Introduction to Unsteady Thermofluid Mechanics", John Wiley and Sons, 1990.
- 19EA-17 R.E. Henry, "Modifications for the Development of the MAAP-DOE Code", DOE/ID-10216 Vol. IV, U.S. Department of Energy, November 1988.
- 19EA-18 S. Levy, "Debris Dispersal from Reactor Cavity During Lower Temperature Simulant Tests of Direct Containment Heating (DCH)", Paper presented at 18th Water Reactor Safety Information Meeting, Gaithersburg MD, NUREG/CP-0114, Volume 2, 1990, pp. 157-206.
- 19EA-19 "An Integrated Structure and Scaling Methodology for Severe Accident Technical Issue Resolution", NUREG-CR 5809, Draft Report for Comment, November 1991.
- 19EA-20 "ABWR Severe Accident Evaluations," UTLR-0014

**Table 19EA-1 Containment Pressure at RPV Failure**

Accident Sequence	Pressure
	MPa
LCLP-PF-D-M	0.13
LCLP-FS-D-L	0.14
LCHP-PS-D-N	0.12
LCHP-PF-P-H	0.12
SBRC-PF-D-H	0.24
LBLC-PF-D-M	0.29
NSCL-PF-D-H	0.13
NSCH-PF-P-H	0.13
NSRC-PF-D-H	0.43

**Table 19EA-2 Comparison of Assumed Debris Mass Participating in DCH with BWRSAR Debris Discharge Results**

Time	Integrated Debris Mass (kg)					
	ABWR DCH Analysis (Minimum Values)			BWRSAR		
	Zr	Metals	Oxides	Zr	Metals	Oxides
Vessel Failure	0	0	0	0	0	0
+2 minutes	6500	*	17,000	926	3880	0
+4 minutes	6500	*	17,000	2316	8172	0

\* Only a small portion of the core plate was assumed to be added to the debris.

**Figure 19EA-1 DCH Event Tree for Sequences with Low Containment Pressure**

Not Part of DCD (Reference 19EA-20)

|

**Figure 19EA-2 DCH Event Tree for Sequences with Intermediate Containment  
Pressure, Not Part of DCD (Reference 19EA-20)**

|

**Figure 19EA-3 DCH Event Tree for Sequences with High Containment Pressure**

Not Part of DCD (Reference 19EA-20)

I



**Figure 19EA-4 DET for Probability of Early Containment Failure—High RV Press  
and Low Cont Press Sequences**

Not Part of DCD (Reference 19EA-20)

I

**Figure 19EA-5 DET for Probability of Early Containment Failure—High RV Press  
and Inter Cont Press Sequences**

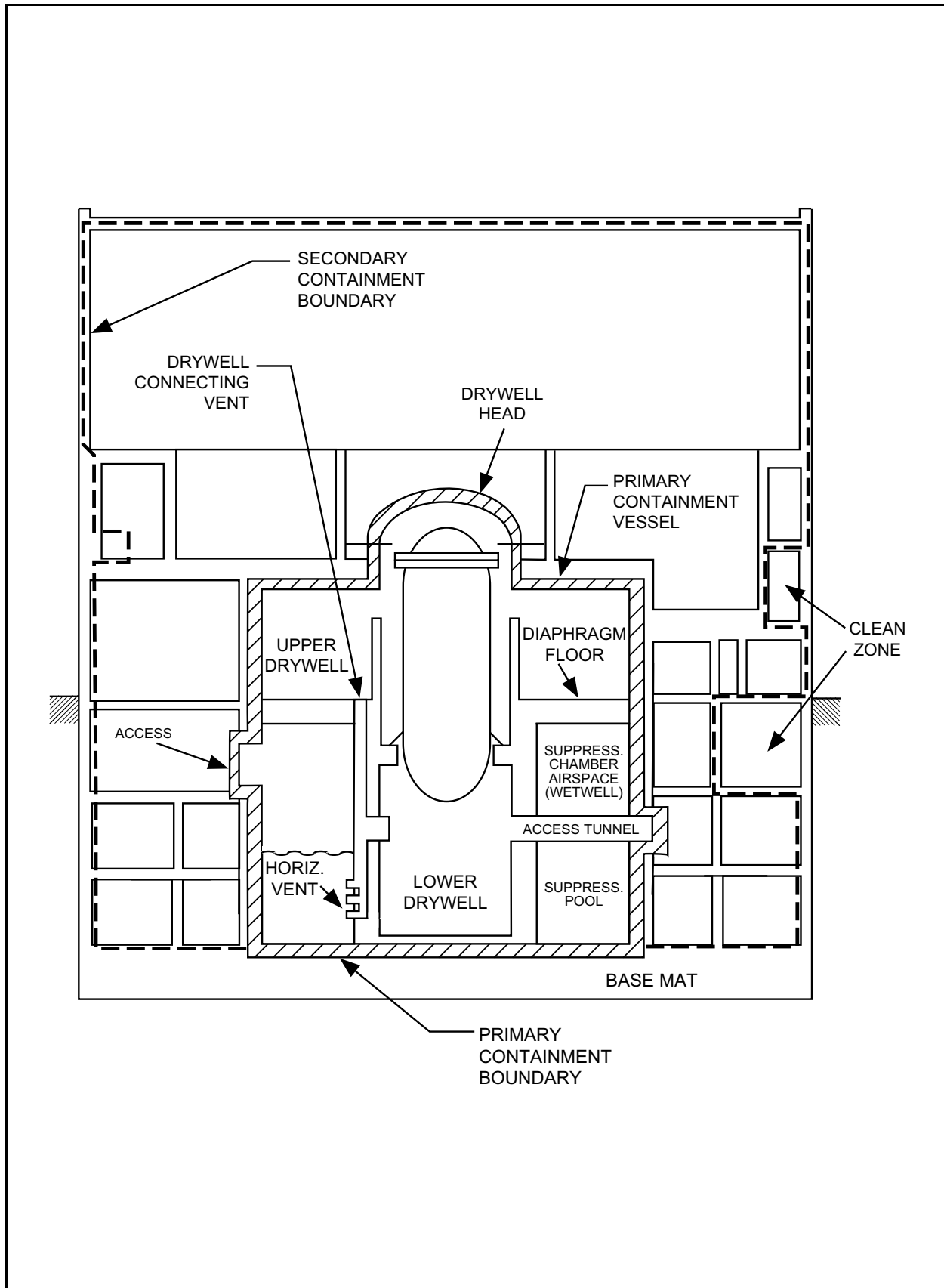
Not Part of DCD (Reference 19EA-20)

I

**Figure 19EA-6 DET for Probability of Early Containment Failure—High RV Press  
and High Cont Press Sequences**

Not Part of DCD (Reference 19EA-20)

I

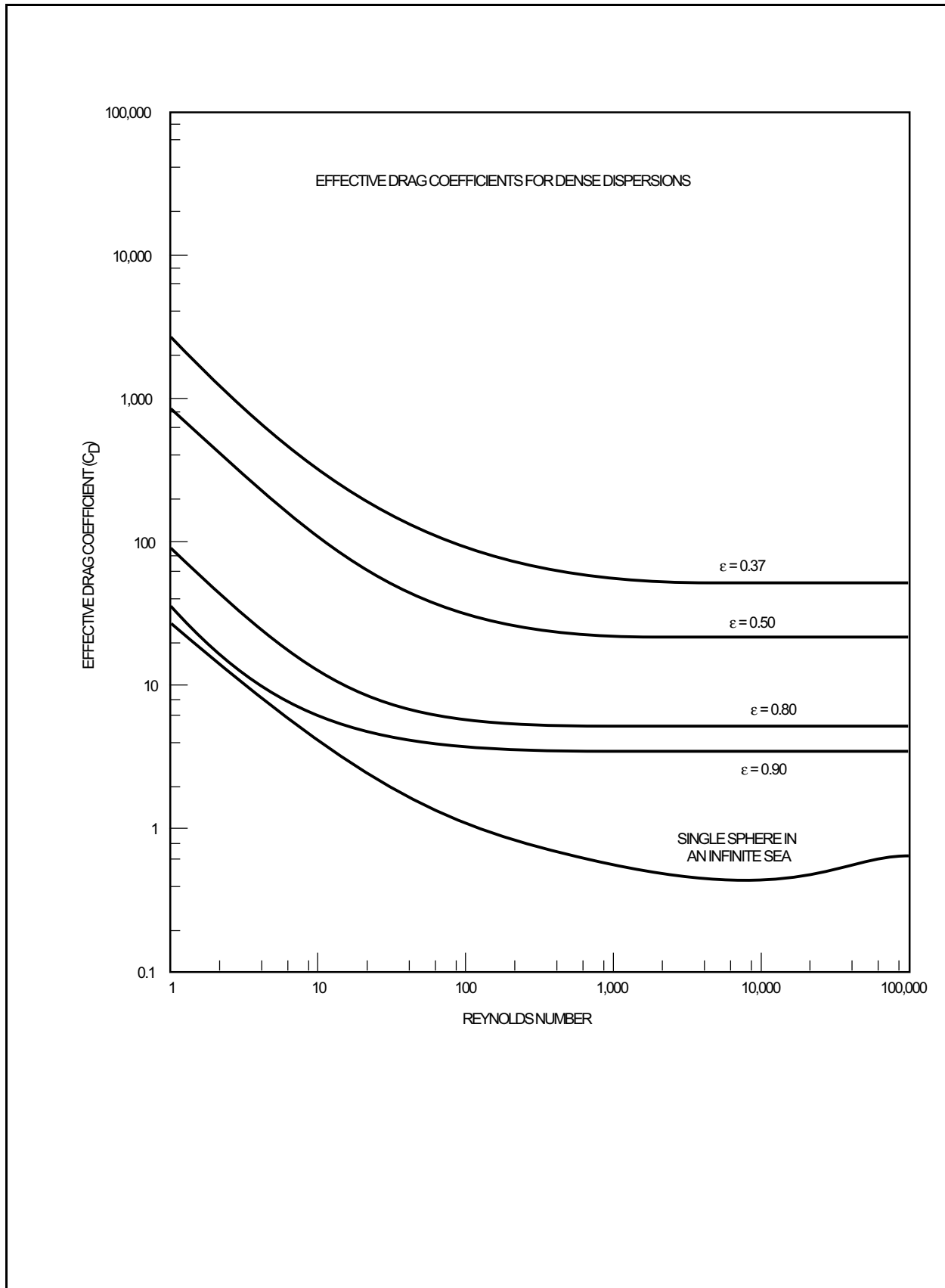
**Figure 19EA-7 ABWR Containment Boundary Nomenclature**

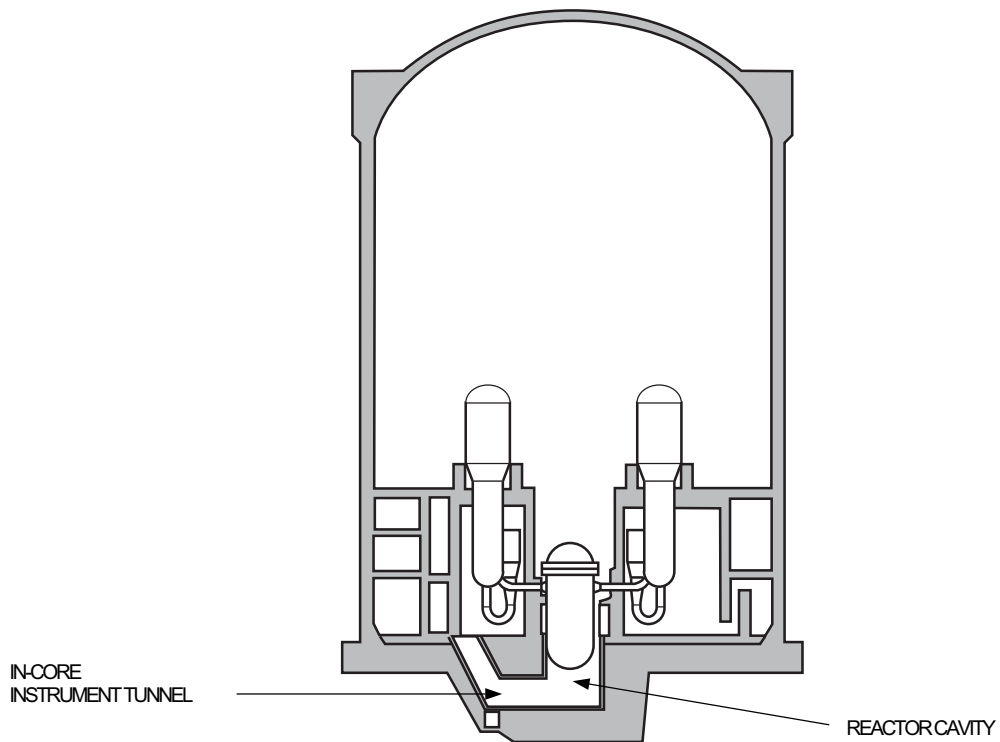
**Figure 19EA-8 Not Used**

**I**

**Figure 19EA-9 Not Used**

**I**

**Figure 19EA-10 Effective Drag Coefficient for Dense Dispersions**

**Figure 19EA-11 Zion Reactor Building**



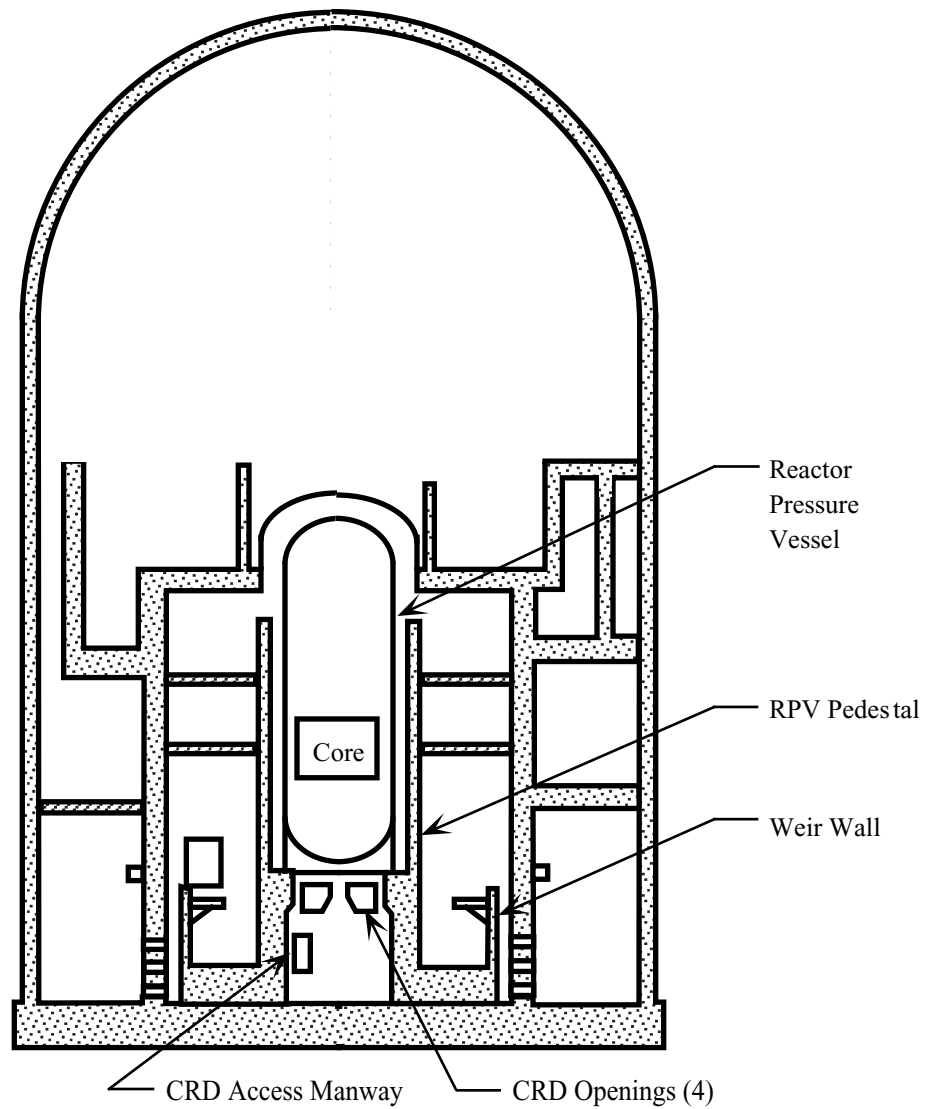


**Figure 19EA-12 Schematic of Grand Gulf Containment**

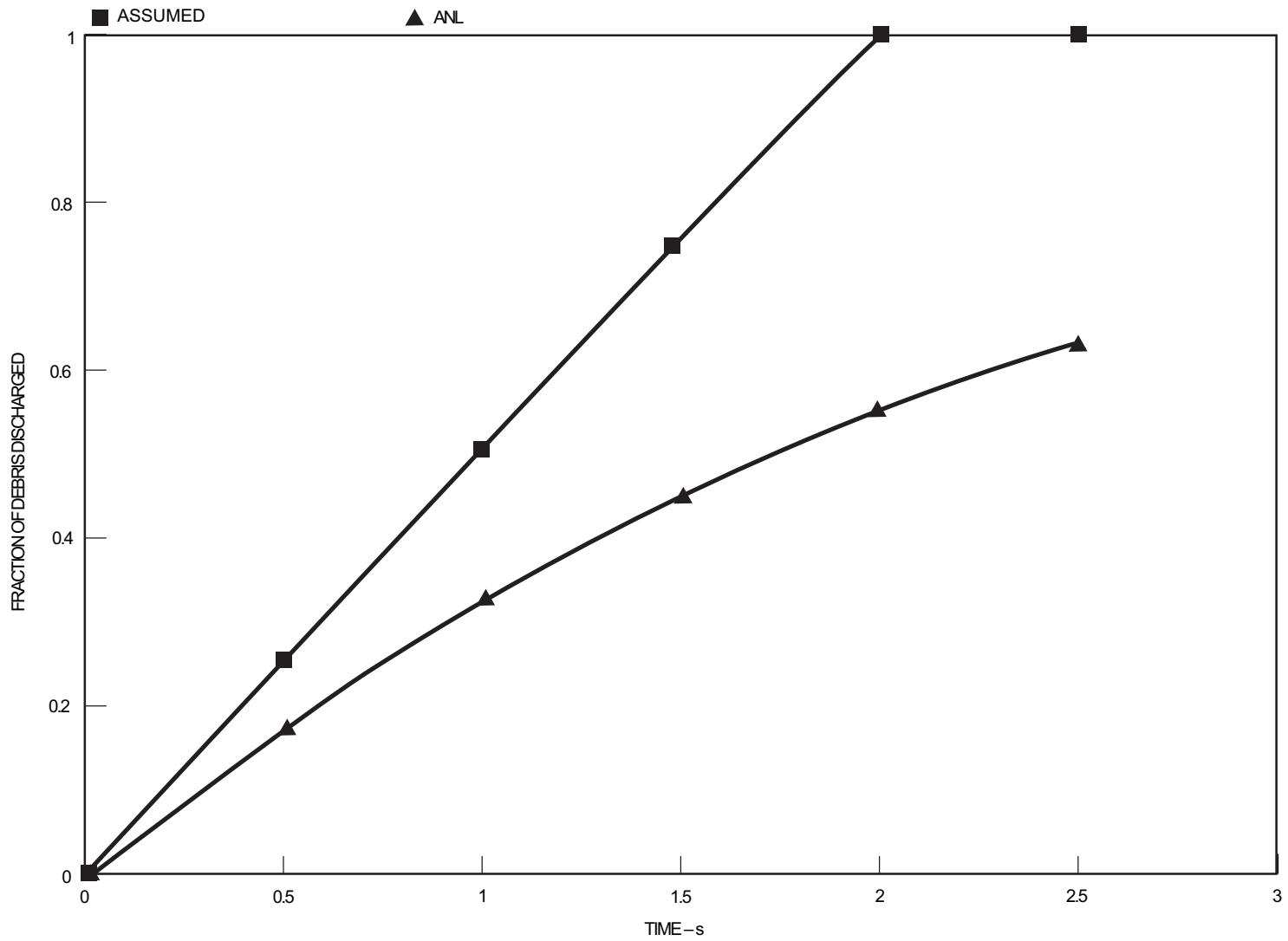


Figure 19EA-13 Comparison of Assumed Debris Discharge to ANL Data Fit

**Figure 19EA-14 Cumulative Distribution for Peak Pressure Due to DCH  
Not Part of DCD (Reference 19EA-20)**

|

**Figure 19EA-15 Not Used**

|